

Shortwave aerosol radiative forcing over cloud-free oceans from Terra: 1. Angular models for aerosols

Jianglong Zhang^{1,2} and Sundar A. Christopher

Department of Atmospheric Sciences, University of Alabama, Huntsville, Alabama, USA

Lorraine A. Remer and Yoram J. Kaufman

NASA Goddard Space Flight Center Data Center, Greenbelt, Maryland, USA

Received 12 May 2004; revised 18 August 2004; accepted 1 December 2004; published 9 March 2005.

[1] Using multiple satellite instruments, we demonstrate a new empirical method for obtaining shortwave (SW) aerosol angular distribution models (ADMs) over cloud-free oceans. We use nearly a year's worth of multispectral Moderate Resolution Imaging Spectroradiometer (MODIS) data to obtain aerosol properties within a Clouds and Earth Radiant Energy System (CERES) footprint and Special Sensor Microwave Imager (SSM/I) data to obtain near surface wind speed. The new aerosol ADMs are built as functions of near-surface ocean wind speed and MODIS aerosol optical depth at 0.55 μm ($\tau_{0.55}$). Among the new features are ADMs as a function of the ratio of fine mode to total aerosol optical depth (η), which contains information on aerosol type, and the combination of the CERES rotation azimuth plane scan mode CERES data and MODIS aerosol products to characterize aerosol properties over glint regions. The instantaneous aerosol forcing efficiencies (SW flux per unit optical depth at $\tau_{0.55}$) are 80.5, 63.1, and 73.0 Wm^{-2} , derived using the Earth Radiation Budget Experiment (ERBE), Tropical Rainfall Measuring Mission (TRMM), and the current Terra ADMs, respectively. This study highlights the necessity for building empirical aerosol ADMs as a function of wind speed, $\tau_{0.55}$ and η , and gives examples of newly constructed aerosol ADMs over cloud-free oceans. We conclude that an overall uncertainty of 10% will be introduced in the derived SW aerosol direct forcing over cloud-free oceans if the ADMs are constructed without considering aerosol darkening effect over glint regions and aerosol brightening over nonglint regions (like ERBE ADMs) or the variations in aerosol properties (like TRMM ADMs). In a companion paper (Zhang et al., 2005), these new ADMs are used to calculate the shortwave aerosol radiative forcing over the global oceans.

Citation: Zhang, J., S. A. Christopher, L. A. Remer, and Y. J. Kaufman (2005), Shortwave aerosol radiative forcing over cloud-free oceans from Terra: 1. Angular models for aerosols, *J. Geophys. Res.*, 110, D10S23, doi:10.1029/2004JD005008.

1. Introduction

[2] The Earth Radiation Budget Experiment (ERBE) and the Clouds and Earth's Radiant Energy System (CERES), were designed to monitor the top of atmosphere (TOA) shortwave (SW) and longwave (LW) radiative energy fluxes of the Earth-atmosphere system [Wielicki et al., 1996]. Among many successful implementations of CERES and ERBE data, include the study of shortwave aerosol direct radiative forcing (SWARF) [Satheesh and Ramanathan, 2000; Loeb and Kato, 2002; Christopher et al., 2000; Christopher and Zhang, 2002a, 2004]. This approach is very similar to the cloud radiative forcing concept [Ramanathan

et al., 1989] wherein if aerosols are properly identified, the difference in TOA fluxes between clear and aerosol regions is called SWARF. Compared to traditional approaches that estimate aerosol forcing using radiative transfer calculations [Chou et al., 2002; Boucher and Tanré, 2000; Christopher and Zhang, 2002b], the distinct advantage of our approach is that it is a measurement based analysis, requiring less assumptions on aerosol properties, and thereby allowing uncertainties to be assessed [Zhang et al., 2005].

[3] Broadband instruments such as the CERES, do not measure outgoing radiative fluxes directly. The angular distribution models (ADMs), that represent the angular characteristics of TOA SW radiances, are used to invert the radiances observed at narrow solid angles to hemispherical fluxes. The ADMs are represented by the anisotropic factor (\mathbf{R}) at specific viewing geometry, and is defined as the ratio between the assumed Lambertian and the actual fluxes [Suttles et al., 1988]. The ADMs are known to be one of the largest uncertainties in deriving TOA fluxes from

¹Now at Naval Research Laboratory, Monterey, California, USA.

²Visiting scientist from University Corporation for Atmospheric Research, Boulder, Colorado, USA.

broadband instruments [Wielicki *et al.*, 1996], and are also one of the largest uncertainties in SWARF studies that use ERBE/CERES measurements [Loeb and Kato, 2002]. The angular characteristics of the TOA outgoing radiation fields are dependent on the observed scene, and are shown to be sensitive to both the cloud optical properties and surface characteristics [e.g., Loeb *et al.*, 2003]. Moreover, both theoretical calculations [Li *et al.*, 2000] and empirical analysis also show that the angular characteristics of reflected SW radiances are sensitive to aerosols and their optical properties. Therefore, to accurately study SWARF using broadband observations, it is necessary to develop ADMs over cloud-free oceans that account for the variations in TOA SW radiation fields due to aerosols.

[4] The commonly used shortwave ADMs are from the ERBE program that was constructed for 12 different scene types [Suttles *et al.*, 1988]. Over oceans, the ERBE ADMs are defined for four different scene types: clear, partially cloudy, mostly cloudy and overcast skies. However, due to the large footprint of ERBE pixels, accurate identification of scene types was not possible and no aerosol identification was included. Recently, new ADMs have been developed using spatially and temporally collocated VIRS and CERES measurements from the Tropical Rainfall Measuring Mission (TRMM) platform although the majority of the emphasis is on clouds [Loeb *et al.*, 2003]. The CERES on TRMM has a spatial resolution of about 10 km at nadir while the VIRS instrument has a much finer spatial resolution of 2 km. Therefore, using collocated VIRS observations, the scene identification capability for the CERES pixels was improved [Loeb *et al.*, 2003]. For example, over cloudy regions over oceans, the TRMM SW ADMs were created for more than ten cloud optical depth and cloud fraction ranges [Loeb *et al.*, 2003]. Over cloud-free oceans, the TRMM ADMs were constructed as a function of wind speed, using the European Centre for Medium-Range Weather Forecasts (ECMWF) data, and account for the aerosol effect using theoretical model calculations by assuming only one maritime tropic aerosol model [Hess *et al.*, 1998], with a high single scattering albedo of 0.998 at 0.55 μm [Loeb and Kato, 2002].

[5] One major difficulty that prevents the construction of empirical aerosol ADMs from TRMM is that the CERES was not designed for aerosol retrievals and therefore relies on narrow band instrument such as the VIRS to identify aerosol properties within a CERES footprint. However, the VIRS has limited number (5) of spectral channels with only one channel (0.63 μm) that is assumed to be sensitive to all aerosol types. Additionally, the VIRS has a larger footprint of about 2 km compared with current satellite instruments like the MODIS (250 to 1 km), and therefore is not best suited for aerosol studies and since the VIRS observes only within $\pm 37^\circ$ latitude it does not provide global data.

[6] The recently launched Terra and Aqua satellites provide a good opportunity for studying the effect of aerosols on the angular distribution pattern of TOA SW fluxes. Both the Terra and Aqua include a narrowband instrument (MODIS), as well as a broadband instrument (CERES). The MODIS instrument has advanced multispectral (36 channels) capabilities with improved spectral, spatial and radiometric resolution when compared with previous imagers [King *et al.*, 1992] and has been used to

detect aerosols, retrieve aerosol optical depth and particle size information [Tanré *et al.*, 1997]. Recent studies have shown that MODIS provides more accurate retrievals of aerosol optical thickness (AOT) when compared to previous imagers such as the AVHRR [e.g., Remer *et al.*, 2002; Chu *et al.*, 2002].

[7] In this study, we used the CERES Single Scanner Footprint (SSF) data, which contains collocated CERES and MODIS observations, to construct aerosol SW ADMs over cloud-free oceans. For regions with $\tau_{0.55} < 0.2$, the aerosol ADMs were built not only as a function of $\tau_{0.55}$ but also as a function of near surface wind speed derived from SSM/I measurements. For $\tau_{0.55} > 0.2$, the aerosol ADMs were built as functions of $\tau_{0.55}$ and fraction of fine mode to total aerosol optical depth (η) [Tanré *et al.*, 1997; Kaufman *et al.*, 2005]. The η parameter has tremendous potential for separating dust from other aerosols [Kaufman *et al.*, 2005; Christopher and Zhang, 2004], and is used to account for the variations in aerosol optical properties to the anisotropy of the reflected SW energy. However, there are no MODIS aerosol retrievals available within 40° glint angles over oceans where the surface reflectance is high [Tanré *et al.*, 1997]. This poses a problem because when constructing aerosol ADMs, aerosol properties for CERES observations at all angles including glint regions are needed. To overcome this issue, two steps were taken in this study. First, the CERES rotational azimuth plan (RAP) scan mode data are used because it has different viewing geometry when compared with the cross track MODIS scanner. Therefore, for a given region over cloud-free oceans, for the RAP scan mode, CERES could scan at a glint angle (ψ) $< 40^\circ$ while the MODIS scans at $\psi > 40^\circ$ and therefore has valid aerosol retrievals for the same region. Therefore the combination of the MODIS and CERES RAP data could provide both radiance and aerosol information for CERES observations within 40° glint angles. Second, within 20° glint angles, only limited RAP pixels are available. Therefore monthly and daily MODIS aerosol products are used in estimating aerosol optical properties over CERES glint regions, and since this is an approximation, the uncertainties in using the MODIS daily aerosol product is described in detail in section 3.

2. Data

[8] Four different data sets from November 2000 to August 2001 are used in this study. The Terra CERES Single Satellite Footprint (SSF) data are used to provide instantaneous broadband SW radiance and collocated MODIS aerosol optical properties including $\tau_{0.55}$ and η and the SSM/I data are used for obtaining near surface wind speed values. The SSF product collocates the CERES with MODIS observations using the CERES point spread function (PSF) where the MODIS derived aerosol and cloud properties are averaged (using point spread function weighting) within a CERES pixel [Loeb and Kato, 2002].

[9] In the MODIS aerosol retrieval algorithm over oceans, aerosols are assumed to have a bimodal distribution [Tanré *et al.*, 1997]. The $\tau_{0.55}$ is assumed to be the result of two aerosol modes: the fine mode that largely represents aerosols from anthropogenic sources and gas-to-particle conversions, and the large mode which largely represents sea salt and dust

aerosols [Tanré et al., 1997]. Compared to ground measurements, the uncertainties in $\tau_{0.55}$ are estimated to be $\pm 0.03 \pm 0.05\tau$ over the ocean [Remer et al., 2002].

[10] Since wind speed is also an important factor affecting the angular characteristics of TOA SW radiances over oceans [Loeb and Kato, 2002], the near-surface wind speed is obtained from the DMSP Special Sensor Scanning Microwave Imager (SSM/I) data product averaged over $0.5^\circ \times 0.5^\circ$ [Wentz, 1997]. Since there is only a one-hour time gap between the DMSP F15 and Terra, we use the DMSP F15 descending overpass data combined with DMSP-14 data set to fill data gaps.

3. Methods

[11] Figure 1a shows glint angle (ψ) versus the TOA CERES radiance over cloud-free global oceans for four $\tau_{0.55}$ ranges (0.0–0.1, 0.1–0.2, 0.2–0.4 and 0.4–0.6) for viewing zenith angles (θ) $< 50^\circ$ and solar zenith angles (θ_0) between 36° – 60° where glint angle (ψ) is defined as the angle between the light beams of real and mirror reflection. Only pixels that have $\eta < 0.9$ and $\tau_{0.55} < 2$ are used. For $\psi > 15^\circ$, the CERES SW radiance increases as $\tau_{0.55}$ increases, that is called aerosol brightening effect. For $\psi < 15^\circ$, as $\tau_{0.55}$ increases, the SW radiance decreases which is called the aerosol darkening effect over glint regions, where aerosols absorb or scatter solar energy thereby reducing the reflectivity of glint regions [Kaufman et al., 2002]. As $\tau_{0.55}$ increases, the TOA angular distribution pattern also changes significantly (1a). Since the TOA SW flux is defined as the integration of radiances at all angles from a reflecting surface, without using aerosol ADMs and without considering aerosol darkening effect over glint regions and aerosol brightening effect over nonglint regions (e.g., ERBE ADMs), the retrieved SWARF, that is defined as the difference between clear and aerosol fluxes [Christopher and Zhang, 2002a], will be overestimated at off-glint angles and underestimated within the glint regions.

[12] Figure 1b shows ψ versus CERES radiance for four wind speed ranges (0–6, 6–9, 9–12 and 12–40 m s^{-1}) and for $\tau_{0.55} < 0.1$. For $\psi > 30^\circ$, there are no significant differences among the SW radiance for the four wind speed ranges. However, for $\psi < 20^\circ$, the SW radiance increases rapidly as wind speed decreases. For example, at $\psi = 5^\circ$, the mean SW radiance decreases from $150 \text{ Wm}^{-2} \text{ sr}^{-1}$ over regions with 0–6 m s^{-1} near surface wind speeds to $70 \text{ Wm}^{-2} \text{ sr}^{-1}$ over regions with wind speeds $> 12 \text{ m s}^{-1}$ indicating the importance of wind speeds on clear sky ADMs over the oceans. Therefore to accurately invert CERES measured SW radiances into TOA flux, it is necessary to separate clear sky ocean ADMs as a function of $\tau_{0.55}$ and near surface wind speeds. Therefore, for $0 < \tau_{0.55} < 0.2$, the ADMs were constructed as functions of both $\tau_{0.55}$ and wind speed and for $\tau_{0.55} > 0.2$ the ADMs were also built as functions of aerosol properties.

[13] The empirical aerosol SW ADMs are created for three $\tau_{0.55}$ ranges (0–0.1, 0.1–0.2 and 0.2–0.4). Between $\tau_{0.55}$ ranges of 0–0.1 and 0.1–0.2, the aerosol ADMs are created for four wind speed ranges (0–6, 6–9, 9–12 and 12–40 m s^{-1}); and for $0.2 < \tau_{0.55} < 0.4$, the aerosol ADMs are for two η ranges; $\eta < 0.6$ and $\eta > 0.6$ [Kaufman et al., 2005; Christopher and Zhang, 2004].

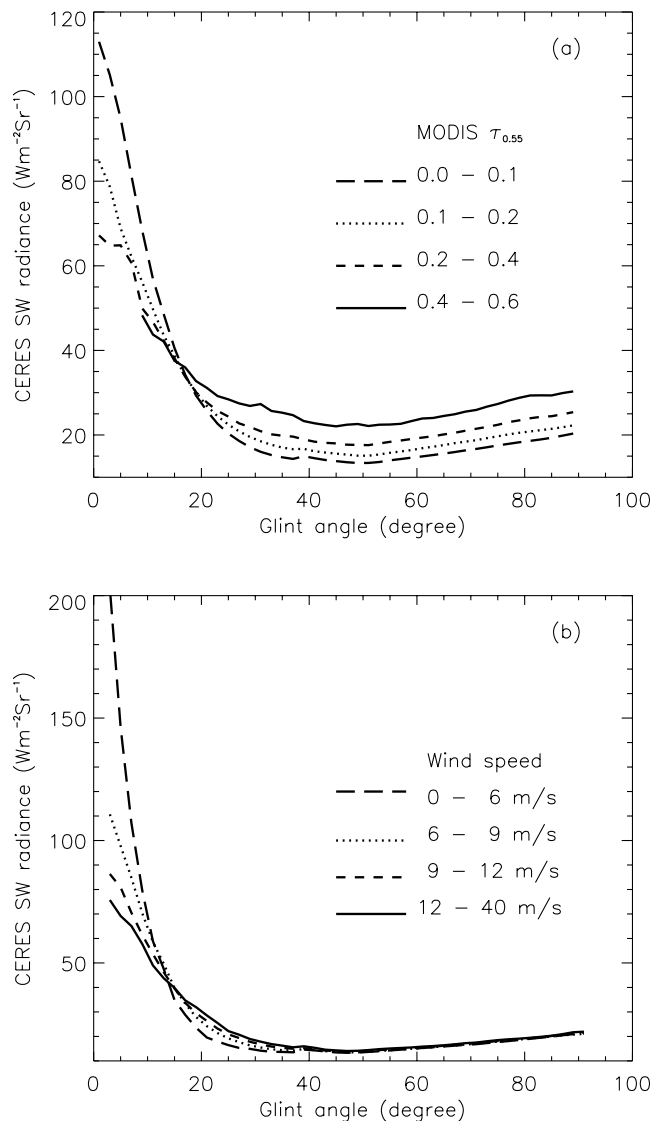


Figure 1. (a) The CERES SW radiance versus glint angle for five MODIS $\tau_{0.55}$ ranges and (b) for four wind speed ranges for $0.0 < \tau_{0.55} < 0.1$.

[14] According to our analysis, for a total of 10 months data, there are less than 2% CERES cloud-free pixels over oceans with $\tau > 0.4$. Therefore, for $\tau > 0.4$, there are not enough pixels to build empirical ADMs, and therefore the 6S model [Vermote et al., 1997] is used to create theoretical clear sky ocean ADMs as a function of τ at nine optical depths (0.3, 0.5, 0.8, 1.0, 1.25, 1.5, 2.0, 2.5 and 3 at $0.55 \mu\text{m}$). An oceanic aerosol model is used [Vermote et al., 1997], and a wind speed of 7.5 m s^{-1} is assumed. For a given CERES observation that have MODIS $\tau > 0.4$, the ratio of theoretically calculated anisotropic factors at MODIS retrieved τ (for $\tau = 0.3$) are computed. The anisotropic factor is then obtained by multiplying the empirical anisotropic factor from Terra aerosol ADMs at τ range of 0.2–0.4 with the modeled ratio.

[15] To be consistent with the TRMM ADMs, the new Terra aerosol ADMs are created for 9 viewing zenith angle (θ) bins, 10 azimuth angle (φ) bins (0° – 9° , 9° – 30° , 30° – 50° , 50° – 70° , 70° – 90° , 90° – 110° , 110° – 130° , 130° –

Table 1. Uncertainties in ADMs Induced From Using Monthly and Daily Mean MODIS AOT

τ	Using Daily Mean τ			Using Monthly Mean τ		
	Frequency, %	Uncertainty, %	Frequency Weighted Uncertainty, %	Frequency, %	Uncertainty, %	Frequency Weighted Uncertainty, %
0.0–0.1 (0–6 m/s)	13	1	0.1	14	1	0.1
(6–9 m/s)	10	0	0	12	0	0
(9–12 m/s)	9	0	0	13	0	0
(12–40 m/s)	7	0	0	19	2	0.4
0.1–0.2 (0–6 m/s)	13	1	0.1	44	8	3.5
(6–9 m/s)	13	1	0.1	35	6	2.1
(9–12 m/s)	12	1	0.1	29	3	0.9
(12–40 m/s)	9	1	0.1	27	1	0.3
0.2–0.4 ($\eta < 0.6$)	16	1	0.1	39	6	2.3
0.2–0.4 ($\eta > 0.6$)	11	1	0.1	30	7	2.1

150°, 150°–171°, 171°–180°), and five solar zenith angle bins (cosine θ_0 values of 1–0.9, 0.9–0.8, 0.8–0.7, 0.7–0.6, 0.6–0.5). Since there are not enough observations for $\theta_0 > 60^\circ$, the ADMs are built only up to 60° θ_0 . For CERES pixels that have $\theta > 80^\circ$, the pixel footprints cover areas beyond the Earth’s tangential point [Loeb *et al.*, 2003] and the scene identifications are unreliable. Since CERES SW radiances from all angular bins are needed, for angular bins with $\theta > 80^\circ$ (which accounts for 11% of the total angular bins), theoretical calculations from the 6S radiative transfer model are used. An oceanic aerosol model is assumed [Vermote *et al.*, 1997]; viewing geometry is set to center value of each angular bin, and the wind speed is set to the mean speed of each wind speed range that was previously indicated.

[16] The CERES pixels that are at least 99.9% cloud-free as defined by MODIS are sorted. The averaged radiance of an angular bin, however, may not represent the bin average value. For example, for the angular bin within the θ_0 range of 36° – 45° , data samples could cluster around a small θ_0 range of (e.g., θ_0 of 36° – 37°). Therefore, for this case, the bin-averaged radiance is biased toward the lower end of the solar zenith angle bin. To account for this effect, each angular domain (θ_0 , θ , φ) is divided into 8 equally spaced subangular domains (1/2 the size of θ_0 , θ and φ bin). The CERES SSF cloud-free data are sorted into the subangular domains, and the average of the 8 radiance values from subangular domains is used to represent the mean value for the angular domain. In this study, we require at least 90% of the angular bins (for $\theta < 80^\circ$) to have a valid entry. A valid entry is defined as having data in 4 out of 8 subangular bins.

[17] There are two problems associated with obtaining the bin-averaged values in each subangular domain. First, over MODIS glint regions ($\psi < 35^\circ$), there is no instantaneous aerosol retrieval from MODIS. Furthermore, the use of SSF rotational azimuth plane (RAP) scan mode data provide only limited data samples over these regions. To obtain enough samples at the angular bins within the MODIS glint regions, one approach would be to approximate aerosol optical properties of CERES pixels over these regions using either the MODIS daily or monthly gridded product. However, the monthly or daily gridded aerosol product may not represent the true instantaneous aerosol information for a given scene. To test the uncertainties associated with the use of gridded aerosol product, for each aerosol optical thickness range (0–0.1, 0.1–0.2, 0.2–0.4) and for each subangular bin in ADMs, bin-averaged radiances derived from

gridded aerosol product are compared with bin-averaged radiances derived from the instantaneous aerosol product (Table 1). Table 1 lists the frequency of angular bins that use instantaneous, daily and monthly mean MODIS data for three sets of aerosol ranges 0.0–0.1, 0.1–0.2 and 0.2–0.4. Also listed in Table 1 are the relative uncertainties in the bin-averaged CERES radiance due to the use of gridded aerosol product. The relative uncertainty is defined as the mean difference between the bin-averaged CERES radiance estimated using instantaneous and gridded aerosol product. Angular bins are selected in this comparison if the difference in bin-averaged θ_0 , θ and φ are less than 2° . Multiplying frequency with the uncertainties, Table 1 shows that the uses of MODIS daily mean τ could induce 0–0.1% uncertainties while the use of MODIS monthly mean τ could induce 0–4% uncertainties in the bin averaged CERES SW radiances for ADMs that are built for 0–0.1, 0.1–0.2 and 0.2–0.4 τ ranges.

[18] Second, even with the use of MODIS daily and monthly gridded product, not every subangular bin has enough data samples, and the average values could be irregularly spaced at the subangular domains. Therefore the Shepard method [Amidror, 2002] is used to interpolate irregularly spaced data into the center of each subangular domain and the aerosol ADMs are created by integrating the bin-averaged radiances at all angular domains.

4. Results

[19] To demonstrate the effect of aerosol optical properties and wind speed on ADMs, Figures 2a–2d show examples of aerosol ADMs for $0.0 < \tau_{0.55} < 0.1$ for four wind speed ranges (0–6, 6–9, 9–12, 12–40 m s^{−1}); Figures 2e–2h for $0.1 < \tau_{0.55} < 0.2$ for the same four wind speed ranges, and Figure 2i for $0.2 < \tau_{0.55} < 0.4$ and $\eta < 0.6$, and Figure 2j for $0.2 < \tau_{0.55} < 0.4$ and $\eta > 0.6$ respectively. The solar zenith angle range is between 0° and 25° . The radius of the polar plot represents the satellite viewing zenith angle, and the polar angle represents the relative azimuth. The center of the polar plot is at satellite nadir view ($\theta = 0^\circ$) and Sun is located at $\varphi = 180^\circ$.

[20] Figures 2a–2d shows the effect of near surface ocean wind speed on the angular distribution pattern of TOA SW radiance. All four figures share the common feature, i.e., the glint region with maximum **R** values are located around 0° – 25° θ and near 0° φ . As wind speed increases from 0–6 to 12–40 m s^{−1}, the **R** values at the glint region decreases

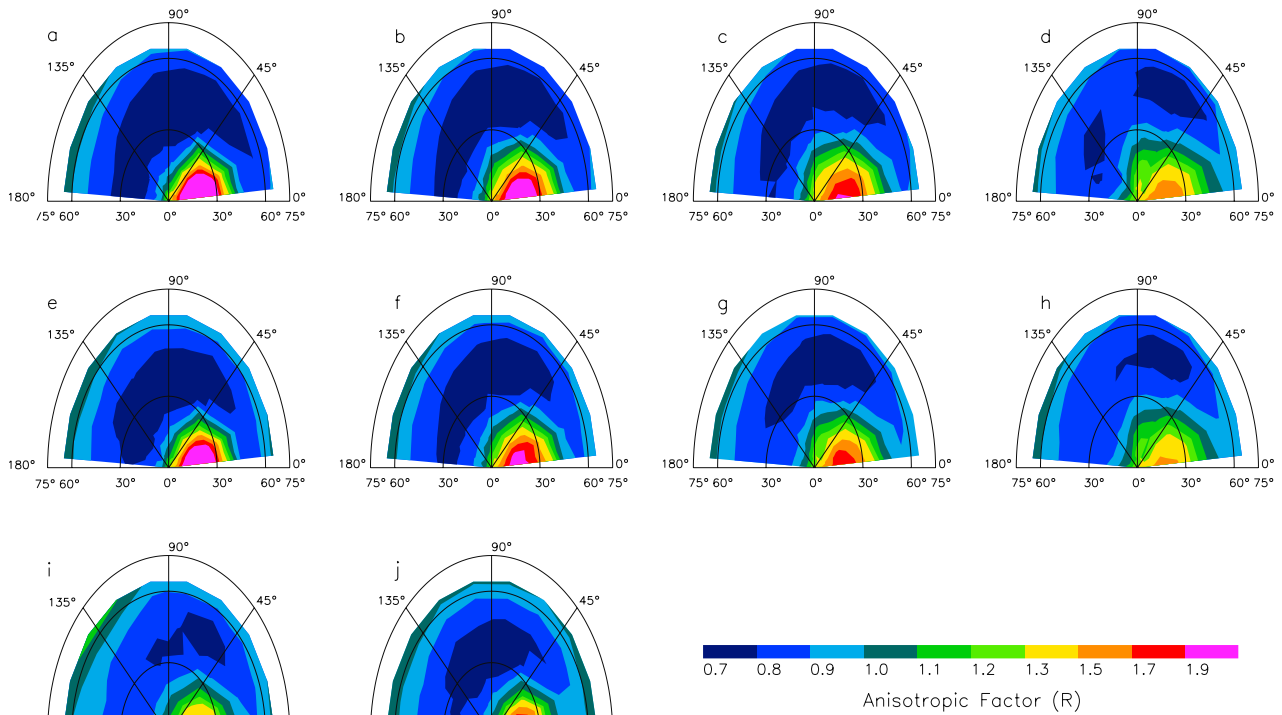


Figure 2. Cloud-free shortwave ADMs over global oceans for $0.9 < \cos \theta_0 < 1.0$ (a–d) for four wind speed ranges of 0–6, 6–9, 9–12 and 12–40 m s^{-1} and for $0.0 < \tau_{0.55} < 0.1$; (e–h) four wind speed ranges of 0–6, 6–9, 9–12 and 12–40 m s^{-1} and for $0.1 < \tau_{0.55} < 0.2$; for (i) $0.2 < \tau_{0.55} < 0.4$ and $\eta < 0.6$; and (j) for $0.2 < \tau_{0.55} < 0.4$ and $\eta > 0.6$.

while the glint regions broaden. Outside the glint regions, the R values in the forward direction ($\varphi < 90^\circ$) increases as wind speed increases while the R values in the reverse direction ($\varphi > 90^\circ$) decreases as wind speed increases. For example, for $\theta = 55^\circ$, the R value increases from 0.83 to 0.98 for $\varphi = 4.5^\circ$ for wind speed changes from 0–6 to 12–40 m s^{-1} and decreases from 0.95 to 0.93 for the same wind speed changes at $175^\circ \varphi$.

[21] These variations in Sun glint and non-Sun-glint angular regions as a function of wind speed can be explained by the interactions between surface winds and ocean surfaces. When near surface ocean wind speeds are less than 3 m s^{-1} , the ocean surfaces are relatively “flat,” and reflect sunlight like a mirror that is called specular reflection. The specular reflection of the Sun would be observed at near $0^\circ \varphi$ and at the viewing zenith angle that is close or equal to the solar zenith angle. At higher wind speeds, waves and whitecaps are formed [e.g., Cox and Munk, 1954; Moore et al., 2000], and ocean surfaces do not behave as a single mirror-like reflector. Ocean surfaces can therefore be pictured as a composite of many small water facets [Cox and Munk, 1954] that reflect sunlight at all directions. Therefore the reflectance values at the glint angles are weakened. Similarly, sunlight could be specularly reflected by many small water facets to angles that are outside of the Sun glint angle ranges, especially at near $0^\circ \varphi$. Therefore the areas of glint angular regions are broadened.

[22] Figures 2e–2h show wind speed effects on aerosol ADMs for $\tau_{0.55}$ between 0.1 and 0.2. Similar to Figures 2a–2d, the increase in wind speed weakens the intensity in maximum R values over glint regions while

broadening the glint regions. One significant difference between Figures 2a–2d and Figures 2e–2h is that the effect of wind speed on the R value at glint regions is reduced. For example, as wind speed varies from 0–3 to 12–40 m s^{-1} , the R value at the center of the glint region changes from 2.8 to 1.7 for ADMs that have $\tau_{0.55}$ values between 0 and 0.1 and change from 2.6 to 1.6 for ADMs that have $\tau_{0.55}$ values between 0.1 and 0.2. The reduction in R value at glint regions is due to the increase in aerosol loading. As $\tau_{0.55}$ increases, more energy is reflected or absorbed before reaching the ocean surface and therefore, the effect of near-surface wind speed to ADMs is reduced.

[23] To date most angular models over the oceans are characterized only as a function of near-surface wind speed and aerosol optical depth [e.g., Loeb and Kato, 2002]. There are currently no ADMs to separate the CERES radiances as a function of aerosol type. While differentiating between specific aerosol types from multispectral measurements is a difficult task from multispectral measurements alone, the fraction of fine mode aerosols to the total aerosol optical depth (η), is a useful surrogate for aerosol type [Kaufman et al., 2005] since fine mode aerosols such as industrial pollution and biomass burning aerosols are largely anthropogenic and wind driven aerosols such as dust and sea salt are mostly natural aerosols. In this study we have developed a framework for constructing ADMs for two broad η categories ($\eta < 0.6$ and $\eta > 0.6$). Figures 2i and 2j show the aerosol ADMs for two different η regimes. When η increases, the R values at the glint regions are significantly reduced. For $\varphi = 4.5^\circ$ and $\theta = 15^\circ$, R is 1.9 for $\eta > 0.6$ and

1.6 for $\eta < 0.6$. It is also interesting to note that outside glint regions, \mathbf{R} increases when η increases at the forward scattering angles.

[24] Using the new aerosol ADMs, SW fluxes are retrieved by dividing CERES unfiltered radiances with \mathbf{R} values of the observing scenes. Figure 3 shows the mean CERES flux as a function of instantaneous MODIS $\tau_{0.55}$ retrieved using ERBE, TRMM and new Terra aerosol ADMs. Only pixels that have glint angles $>35^\circ$ are selected. The major differences among Terra, TRMM and ERBE ocean clear sky SW ADMs are that ERBE ADMs are only built as a function of viewing geometry, and variations in anisotropic factors due to near surface wind and aerosol loading is not included. The TRMM ADMs are built as a function of ECMWF wind speed (assimilated using SSM/I winds), and account for aerosol effects using theoretical calculations by assuming a maritime tropical aerosol model for all optical depths. In comparison, in this study the Terra ADMs are built as functions of both SSMI near surface wind speed and MODIS retrieved aerosol optical properties.

[25] The use of ERBE ADMs results in the largest slope between MODIS $\tau_{0.55}$ and retrieved CERES flux. Since the SWARF is defined as the difference between CERES flux without and with presence of aerosols, the largest slope implies the largest SWARF for a given $\tau_{0.55}$ value. This indicates that without considering the aerosol-darkening effect over glint regions and the aerosol-brightening over nonglint regions (like ERBE ADMs), the derived SWARF will be overestimated. It is also interesting to note that for a near zero $\tau_{0.55}$ value, the lowest retrieved flux of 66 Wm^{-2} is found when using ERBE ADMs when ERBE SW clear sky ocean ADMs were constructed, partially cloudy (0–5% cloud fraction) pixels were also included [Suttles *et al.*, 1988]. With cloud contamination, the \mathbf{R} values are increased at off-glint regions and correspondingly, the retrieved flux is reduced.

[26] The mean fluxes retrieved from both Terra and TRMM ADMs match when $\tau_{0.55} = 0.26$. For $\tau_{0.55}$ between 0 and 0.26, the SW fluxes retrieved from Terra ADMs are lower than that of TRMM ADMs, whereas for $\tau_{0.55}$ between 0.26 and 0.6, the fluxes retrieved from Terra ADMs are higher than those retrieved by the TRMM ADMs. The slope of $\tau_{0.55}$ versus CERES flux (also known as aerosol forcing efficiency) is lower for TRMM ADMs when compared to Terra ADMs and the differences in slopes can be explained due to the aerosol models used. Recall that in TRMM ADMs, the effect of aerosol optical depth to the TOA radiation field are corrected using one tropical maritime aerosol model [Hess *et al.*, 1998] with single scattering albedos very close to one indicating nonabsorbing aerosols [Loeb and Kato, 2002]. However, note that the maritime aerosols have a small η value on the order of 0.3 [Kaufman *et al.*, 2005]. The new Terra ADMs, however, use MODIS $\tau_{0.55}$ retrievals, and as an example use two groups of η values ($\eta < 0.6$ and $\eta > 0.6$) to represent different aerosols in the troposphere [Christopher and Zhang, 2004]. In this study, for $\tau_{0.55} > 0.2$, nearly 80% of the CERES pixels have η values greater than 0.6. Therefore the use of only the maritime aerosol model in ADMs is not appropriate for representing the mean η value.

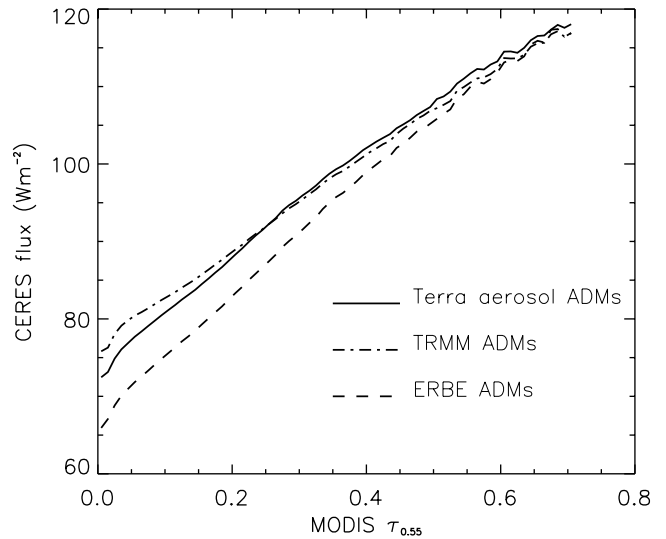


Figure 3. Intercomparison of the mean shortwave flux as a function of $\tau_{0.55}$ derived using ERBE, TRMM and the new Terra ADMs.

[27] To determine if the retrieved TOA SW fluxes are sensitive to ADMs at different η values, we performed flux calculations for all pixels (with $\tau_{0.55} > 0.2$) by using only ADMs from $\eta < 0.6$. We then compared these results to flux calculations using only ADMs from $\eta > 0.6$ and found a 10% underestimation in SWARF for CERES cloud-free oceans pixels. For MODIS $\tau_{0.55} > 0.06$, the column aerosols are a mixture of heterogeneous aerosols such as smoke, polluted aerosol and dust aerosols [Kaufman *et al.*, 2005], and have averaged η values larger than that of marine aerosols. Therefore the use of the maritime tropical aerosol model to correct the aerosol effect at high aerosol loading scene ($\tau_{0.55} > 0.1$) could induce an underestimation in aerosol forcing efficiency (which is proportional to the slope of τ versus CERES flux) as well as the SWARF.

[28] Averaged over 10 months of data, the instantaneous aerosol forcing efficiency (for $\tau_{0.55} < 0.4$) derived using the new Terra ADMs is 73.0 Wm^{-2} per $\tau_{0.55}$, and is bounded by 63.1 and 80.5 Wm^{-2} per $\tau_{0.55}$ that are derived using TRMM and ERBE ADMs respectively. A 10% uncertainty is observed without using the empirical aerosol ADMs that account for the variations of aerosol properties to the TOA radiance fields.

5. Summary

[29] Using collocated MODIS and CERES data we have presented a strategy for developing aerosol ADMs over the global oceans that could be used for aerosol radiative forcing studies. The new aerosol ADMs are constructed as function of $\tau_{0.55}$, near surface wind speed and η . Although previous studies have also developed ADMs as a function of wind speed and aerosol optical depth using one fixed aerosol model [Loeb and Kato, 2002], the current study is a significant improvement because the MODIS aerosol optical depth retrieval algorithm does not assume one fixed aerosol type. The parameter η is used in the new aerosol ADMs to account for the variations in aerosol properties to

the anisotropy of TOA radiance fields that was also not available previously. This factor could provide information on separating dust from other aerosols [Kaufman et al., 2005]. To avoid problems with Sun glint, the combination of CERES RAP data and MODIS aerosol products has been used in studying the TOA radiation field as functions of aerosol properties over glint regions. This study suggests that the shortwave aerosol forcing efficiency and SWARF values derived using ERBE and TRMM ADMs are the lower and upper bounds due to uncertainties in ADMs. The SW aerosol forcing efficiencies (proportional to slope of τ versus CERES flux) are 80.5, 63.1, and 73.0 Wm^{-2} per τ for flux (derived using ERBE, TRMM and new Terra clear sky ocean ADMs respectively). In a companion paper, these new ADMs are used to calculate the SWARF over the global oceans [Zhang et al., 2005].

[30] We note that this is one of the first attempts to build aerosol ADMs from observations as a function of wind speed, AOT and η . However, as satellite retrievals of aerosols continue to mature, ADMs could be built as functions of other properties such as specific aerosol types.

[31] **Acknowledgments.** This research is supported by NASA's Radiation Sciences, EOS Interdisciplinary Sciences, and ACMAP programs. J. Zhang was supported by NASA's Earth System Science Fellowship and Aerocenter visiting scientist programs. The CERES data were obtained from the NASA Langley Research Center Atmospheric Sciences Data Center, the MODIS data were obtained through the Goddard Space Flight Center Data Center, and the SSMI data were obtained from the Global Hydrology and Climate Center in Huntsville, Alabama.

References

- Amidror, I. (2002), Scattered data interpolation methods for electronic imaging systems, A survey, *J. Electron. Imaging*, 11(2), 157–176.
- Boucher, O., and D. Tanré (2000), Estimation of the aerosol perturbation to the Earth's radiative budget over oceans using POLDER satellite aerosol retrievals, *Geophys. Res. Lett.*, 27(8), 1103–1106.
- Chou, M., P. Chan, and M. Wang (2002), Aerosol radiative forcing derived from sea WiFS-retrieved aerosol optical properties, *J. Atmos. Sci.*, 59, 748–757.
- Christopher, S. A., and J. Zhang (2002a), Shortwave aerosol radiative forcing from MODIS and CERES observations over the oceans, *Geophys. Res. Lett.*, 29(18), 1859, doi:10.1029/2002GL014803.
- Christopher, S. A., and J. Zhang (2002b), Daytime variation of shortwave direct radiative forcing of biomass burning aerosols from GOES 8 imager, *J. Atmos. Sci.*, 59(2), 681–691.
- Christopher, S. A., and J. Zhang (2004), Cloud-free shortwave aerosol radiative effect over oceans: Strategies for identifying anthropogenic forcing from Terra satellite measurements, *Geophys. Res. Lett.*, 31, L18101, doi:10.1029/2004GL020510.
- Christopher, S. A., J. Chou, J. Zhang, X. Li, and R. M. Welch (2000), Shortwave direct radiative forcing of biomass burning aerosols estimated from VIRS and CERES, *Geophys. Res. Lett.*, 27, 2197–2200.
- Chu, D. A., Y. J. Kaufman, C. Ichoku, L. A. Remer, D. Tanré, and B. N. Holben (2002), Validation of MODIS aerosol optical depth retrieval over land, *Geophys. Res. Lett.*, 29(12), 8007, doi:10.1029/2001GL013205.
- Cox, C., and W. Munk (1954), Measurements of the roughness of the sea surface from photographs of the Sun's glitter, *J. Opt. Soc. Am.*, 44, 838–850.
- Hess, M., P. Koepke, and I. Schult (1998), Optical properties of aerosols and clouds: The software package OPAC, *Bull. Am. Meteorol. Soc.*, 79, 831–844.
- Kaufman, Y. J., J. V. Martins, L. A. Remer, M. R. Schoeberl, and M. A. Yamasoe (2002), Satellite retrieval of aerosol absorption over the oceans using Sun glint, *Geophys. Res. Lett.*, 29(19), 1928, doi:10.1029/2002GL015403.
- Kaufman, Y. J., I. Koren, L. A. Remer, D. Tanré, P. Ginoux, and S. Fan (2005), Dust transport and deposition observed from the Terra-Moderate Resolution Imaging Spectroradiometer (MODIS) spacecraft over the Atlantic Ocean, *J. Geophys. Res.*, D10S12, doi:10.1029/2003JD004436.
- King, M. D., Y. J. Kaufman, W. P. Menzel, and D. Tanré (1992), Remote sensing of cloud, aerosol, and water vapor properties from the Moderate Resolution Imaging Spectrometer (MODIS), *IEEE Trans. Geosci. Remote Sens.*, 30, 2–27.
- Li, X., S. A. Christopher, J. Chou, and R. M. Welch (2000), Estimation of shortwave direct radiative forcing of biomass-burning aerosols using new Angular models, *J. Appl. Meteorol.*, 39, 2278–2291.
- Loeb, N. G., and S. Kato (2002), Top-of-atmosphere direct radiative effect of aerosols from the Clouds and the Earth's Radiant Energy System Satellite instrument (CERES), *J. Clim.*, 15, 1474–1484.
- Loeb, N. G., et al. (2003), Angular distribution models for Top-of-Atmosphere radiative flux estimation from the Clouds and the Earth's Radiant Energy System instrument on the Tropical Rainfall Measuring Mission satellite. part I: Methodology, *J. Appl. Meteorol.*, 42, 240–265.
- Moore, K. D., K. J. Voss, and H. R. Gordon (2000), Spectral reflectance of whitecaps: Their contribution to water-leaving radiance, *J. Geophys. Res.*, 105, 6493–6499.
- Ramanathan, V., et al. (1989), Cloud-radiative forcing and climate: Results from the Earth Radiation Budget Experiment, *Science*, 6, 57–63.
- Remer, L. A., et al. (2002), Validation of MODIS aerosol retrieval over ocean, *Geophys. Res. Lett.*, 29(12), 8008, doi:10.1029/2001GL013204.
- Satheesh, S. K., and V. Ramanathan (2000), Large differences in tropical aerosol forcing at the top of the atmosphere and Earth's surface, *Nature*, 405, 60–63.
- Suttles, J. T., et al. (1988), Angular radiation models for Earth-atmosphere system. I—Shortwave radiation, *Rep. NASA RP-1184*, 144 pp., NASA, Greenbelt, Md.
- Tanré, D., Y. J. Kaufman, M. Herman, and S. Matto (1997), Remote sensing of aerosol properties over oceans using the MODIS/EOS spectral radiance, *J. Geophys. Res.*, 102, 16,971–16,988.
- Vermote, E., D. Tanre, and J. J. Morcrette (1997), Second simulation of the satellite signal in the solar spectrum 6S: An overview, *IEEE Trans. Geosci. Remote Sens.*, 35(3), 675–686.
- Wentz, F. J. (1997), A well-calibrated ocean algorithm for Special Sensor Microwave/Imager, *J. Geophys. Res.*, 102(C4), 8703–8718.
- Wielicki, B. A., B. R. Barkstrom, E. F. Harrison, R. B. Lee III, G. L. Smith, and J. E. Cooper (1996), Clouds and the Earth's Radiant Energy System (CERES): An Earth Observing System Experiment, *Bull. Am. Meteorol. Soc.*, 77, 853–868.
- Zhang, J., S. A. Christopher, L. A. Remer, and Y. J. Kaufman (2005), Shortwave aerosol radiative forcing over cloud-free oceans from Terra: 2. Seasonal and global distributions, *J. Geophys. Res.*, D10S24, doi:10.1029/2004JD005009.
- S. A. Christopher, Department of Atmospheric Sciences, University of Alabama, 320 Sparkman Drive, Huntsville, AL 35805-1912, USA.
- Y. J. Kaufman and L. A. Remer, Code 913, NASA Goddard Space Flight Center Data Center, Greenbelt, MD 20771, USA.
- J. Zhang, Naval Research Laboratory, 7 Grace Hopper Ave., Stop 2, Monterey, CA 93943-5502, USA. (zhang@nrlmry.navy.mil)